The effects of chemical and mechanical interactions on the thermodynamic pressure for mineral solid solutions

Santiago P. Clavijo[1,*], Luis Espath[2], and Victor M. Calo[3]

[1]Ali I. Al-Naimi Petroleum Engineering Research Center, King Abdullah University of Science and Technology (KAUST),
Thuwal, 23955-6900, Saudi Arabia.
[2]School of Mathematical Sciences, University of Nottingham, Nottingham, NG7 2RD, United Kingdom
[3]School of Electrical Engineering, Computing & Mathematical Sciences, Curtin University, Kent Street, Bentley, Perth, WA
6102, Australia
[*]Corresponding author Santiago P. Clavijo sapenacl91@gmail.com

Key points

1. Phase-field modeling of chemo-mechanical interactions in mineral solid solutions

2. Coupled reactive chemo-mechanical model for multicomponent systems

3. Thermodynamic pressure

Abstract

We use a coupled thermodynamically-consistent framework to model reactive chemo-mechanical responses of solid solutions. Specifically, we focus on chemically active solid solutions that are subject to mechanical effects due to heterogeneous stress distributions. The stress generation process is driven solely by volume changes associated with the chemical processes. We use this model to describe the underlying physics during standard geological processes. Furthermore, simulation results of a three-species solid solution provide insights into the phenomena and verify the interleaving between mechanical and chemical responses in the solid. In particular, we show the evolution of the thermodynamic pressure as the system goes to a steady state.

1 Introduction

In discussing systems undergoing volume changes, Truesdell [39] §5C—in the appendix *A Theory of Multi-phase Mixtures* by Passman, Nunziato & Walsh—identified the thermodynamic pressure as the conjugate power expenditure to volume changes.

The spherical part of the Cauchy tensor only provides mechanical contributions, albeit essential to the thermodynamic pressure. Consequently, the spherical part of the Cauchy tensor does not completely describe the pressure, specially for systems undertaking chemical process. The thermodynamic pressure is defined as the negative variation of the Helmholtz free-energy with respect to the volumetric variations, i.e., $p^{th} = -\partial\psi/\partial v$; this definition automatically satisfies the mechanical version of the second law of thermodynamics. In general, the thermodynamic pressure may be spatially heterogeneous at a steady state and change over time. Therefore, the system reaches equilibrium under non-hydrostatic stresses [21, 22, 23, 20].

This work is part of a series of papers on the chemo-mechanical responses of solid solutions in conjunction with the phase-field model applied to geosystems. Herein, we use the proposed model in Clavijo et al. [6, 7] to assess the chemical contributions to the thermodynamic pressure in a mineral solid solution. Our model, detailed in Clavijo et al. [6, 7], is a thermodynamically-consistent framework for describing chemo-mechanical interactions of solid solutions far from equilibrium.

Our main novel contributions from this work are:

1. Modeling the inhomogeneous pressure distributions that result from local volume changes and showing that species nucleation and growth induce volumetric stresses that lead to spatially inhomogeneous pressure distributions.

2. Demonstrating that mineral solid solutions can reach equilibrium under non-hydrostatic stresses, which has been largely disregarded in the current state of the art.

3. Showing that chemical contributions play a major role in the evolution of these systems, which is an important step in understanding the complex interactions between chemical and mechanical processes in mineral solid solutions.

4. Highlighting the importance of interfacial effects in mineral solid solutions, which have been poorly studied in previous works in the field. Our model takes into account the contribution of interfacial phenomena, such as interfaces between different solid phases, to the overall thermodynamic pressure of the system.

Following Clavijo et al. [6], the elastic energy relates the stress-assisted volume changes and the stresses resulting from mechanical loading. Further, the chemical energy accounts for the interfacial contributions. In particular, we study a solid elastic solution composed of three species. As the species diffuse and react, the solid undergoes volumetric stresses that drive the inhomogeneous pressure distribution. The material parameters in the simulation are in the range of physical and chemical processes in geosciences. We model the elastic properties as a function of the volume fraction, as usually done in the theory of mixtures. We keep the elastic properties constant throughout the simulations without losing generality to model the most straightforward scenario. Thus, we focus on the spatial heterogeneities in the thermodynamic pressure arising from chemical processes.

Studies on metamorphic petrology and microstructural observations suggest the influence of mechanical effects upon chemically active metamorphic minerals. An open research topic in geosciences is to characterize the sources that engender heterogeneous pressure distributions in metamorphic minerals. Most importantly, the pressure conditions that define equilibrium conditions in metamorphic systems. In this effort, several modeling and experimental attempts have been proposed in the literature [27, 38, 15, 30, 41, 42, 43]. Nonetheless, there is a long-standing controversy about the correct magnitude of such pressure distributions predicted by these models. The accuracy of pressure distributions predicted by models is a subject of ongoing research and debate in the scientific community. There are a variety of factors that can affect the predicted pressure distributions, including the complexity of the model, the quality and accuracy of the input data, and the specific assumptions and approximations used in the model. The development of new and improved models, as well as the collection of more accurate data, may help to resolve some of the controversies surrounding pressure predictions. For instance, Tajčmanová et al. [38] study the effects of inhomogeneous pressure distributions and review possible thermodynamic formulations to describe such systems. Their results suggest pressure deviations from lithostatic values larger than 1 GPa even at the micrometre scale. Howell et al. [17] use an analytical model that relates geometric features (host rock and inclusion shapes) in conjunction with quantitative birefringence analysis to study the residual stress of graphite inclusion in a diamond. Their measurements show internal inhomogeneous pressure distributions around graphite inclusions are caused by residual stresses. We do not disregard the possibility of heterogeneous pressures arising from residual stresses caused either by solidification or plastification in conjunction with volume changes induced by chemical processes. However, we restrict attention to volume changes due to chemical reactions to quantify the magnitude of such effects.

To date, a small community has modeled the physical and chemical interactions in mineral mineral solutions. Tajčmanová et al. [38] study the effect of inhomogeneous pressure distributions considering the impact of mass fluxes and external loading, suggesting that a rock composed of two minerals with different mechanical properties will evolve to favor mechanically maintained inhomogeneous pressure distributions. Powell et al. [34] explores incorporating non-hydrostatic thermodynamics to explain observed patterns in metamorphic belts. Their results suggest non-hydrostatic stress in minerals does not significantly affect metamorphism, and commonly adopted approaches in mineral equilibria calculations are unlikely to be affected by non-hydrostatically stressed minerals. According to Powell et al. [34], their conclusions are supported by the success of these calculations in accounting for fundamental patterns in orogens and is inconsistent with a view of metamorphism dominated by non-hydrostatic effects.

To understand the underlying phenomenon leading to inhomogeneous spatial distribution of the thermodynamic pressure, geoscientists must consider all possible mechanisms that favour volumetric deformation. As a part of this effort, this work portraits intrinsic relation between chemo-mechanical responses of mineral solid solutions. The considered framework cannot wholly describe a rock. Rocks are complex systems composed of several minerals and grain boundaries whose crystalline structure and chemical and mechanical properties differ. Moreover, during metamorphism, rocks interact with fluids that strongly define the grade of metamorphism, altering the rock properties. Nevertheless, the aforementioned model sets the basis for a thermodynamical treatment to describe the thermodynamic pressure which defines equilibrium conditions.

The remainder of the paper has the following structure. Section 2 covers a list of dimensionless forms for the coupled chemo-mechanical equations as well as initial and boundary conditions. Section 3 presents the model thermodynamics. Section 3.1 covers the definition of the network model proposed by Larché and Cahn in conjunction with the nature of solidity while allowing for compositional changes, followed by Section 3.3 which describes the elastic energy, particularly the coupling between chemical and mechanical processes. Section 3.4 outlines the definition of a chemical energy potential considering interfacial interactions. We also describe the Ostwald ripening effect and spinodal decomposition processes. Section 3.5 discusses the underlying physics that rules the evolution of elastic solids undergoing chemical processes. In this section, we also show how to calculate the thermodynamic pressure from the Helmholtz free-energy density. Finally, in section 4, we study the evolution of a three-species solid solution where one species results from a forward chemical reaction. Such a coupled chemo-mechanical process drives the generation of the inhomogeneous pressure distributions. Hence, the system reaches equilibrium under inhomogeneous spatial distribution of the thermodynamic pressure.

2 A dimensionless system of coupled chemo-mechanical equations

We adopt the notation proposed by Fried and Gurtin to define a chemical component in saturated systems [14]. The Helmholtz free energy functional accounts for the contributions from the mechanical and chemical responses of the system. Regarding the chemical energy, the functional characterizes a solid system's dynamics that may undergo spinodal decomposition at solid-state, where interfacial interactions drive the spinodal decomposition process. The solid, composed of the several species, is described as a compressible neo-Hookean elastic material. We treat the solid as a continuum body subject to a motion described by a deformation field. The kinematics of the motion of the particles in the body define the deformation field. In the continuum mechanics literature, such systems are commonly called solid-species solutions. Henceforth, we adopt this denomination [14].

A set of balance equations in the form of partial differential equations define how mass, linear and angular momenta, internal energy, and entropy of the system vary in time as deformation and chemical processes take place. As shown in Gurtin et al. [14], Dal and Miehe [8], Miehe et al. [25], Tsagrakis and Aifantis [40], three primary fields govern the coupled chemo-mechanical responses of a solid-species solution: the deformation field, the species concentrations, and the chemical potentials.

The system's total free-energy density characterizes the evolution of elastic solids undergoing chemical processes. This energy potential additively accounts for the elastic and chemical energy densities contributions outlined in Sections 3.3 and 3.4. The total free-energy density reads

$$\hat{\psi} = \hat{\psi}^{ch} + \hat{\psi}^{el}. \tag{1}$$

Conventionally, the chemical energy density can be written as $\hat{\psi}^{ch} = \hat{\psi}^{\varphi} + \hat{\psi}^{s}$, where $\hat{\psi}^{\varphi}$ represents an homogeneous free-energy density and $\hat{\psi}^{s}$ considers interfacial contributions due to concentration gradients. Following Clavijo et al. [5], the chemical energy density used in this work extends to a multi-component framework, the classical free-energy potential used in Cahn-Hilliard formulations [3, 12].

Table 1 summarizes the main governing and constitutive equations; it lists the balance equations, chemical potentials, source/sink terms, and stress tensor for the chemo-mechanical framework proposed in [6, 7].

Lastly, the elastic free-energy density reads

$$\hat{\psi}^{el}(\mathbf{F}^e) = \frac{G}{2}\left[\mathbf{F}^e \colon \mathbf{F}^e - 3\right] + \frac{G}{\beta}\left[(\det\mathbf{F}^e)^{-\beta} - 1\right] \tag{2}$$

Table 1: Coupled system of chemo-mechanical equations

Equation	Description
$\rho_0 = J\rho$	Balance solid mass
$\dot{\varphi}_R^\alpha = s^\alpha - \mathrm{Div}\, \boldsymbol{J}_{R\sigma}^\alpha$	Balance species concentration
$\boldsymbol{J}_{R\sigma}^\alpha = -\sum_{\beta=1}^{n} \boldsymbol{M}^{\alpha\beta}\, J\mathbf{C}^{-1}\nabla\mu_{R\sigma}^\beta$	Species mass flux
$\mu_{R\sigma}^\alpha = \frac{\partial^{(\sigma)}\psi}{\partial\varphi_R^\alpha} - \mathrm{Div}\,\frac{\partial^{(\sigma)}\psi}{\partial(\nabla\varphi_R^\alpha)} - (\gamma^\alpha + \gamma^\sigma)$	Species chemical potential
$s^\alpha = -\sum_{c=1}^{N_s}(v_{\alpha c} - \varpi_{\alpha c})(k_c^+ \prod_{a=1}^{n}(\varphi_R^a)^{v_{ac}} - k_c^- \prod_{a=1}^{n}(\varphi_R^a)^{\varpi_{ac}})$	Chemical reaction source term
$\mathbf{0} = \mathrm{Div}\,\mathbf{T}_R + \mathbf{b}$	Balance linear momentum
$\mathbf{T}_R = G\mathrm{J}_\varphi^{-1/3}[\mathbf{F}^e - (\det\mathbf{F}^e)^{-\beta}\mathbf{F}^{e-\top}]$	Stress tensor
$\mathrm{J}_\varphi = \left(1 + \sum_{\alpha=1}^{n}\omega^\alpha(\varphi_R^\alpha - \varphi_{R0}^\alpha)\right)$	Chemical volumetric deformation
$p^{th} = -\frac{\partial\psi}{\partial v} = -\rho_0\frac{\partial\psi}{\partial J}$	Thermodynamic pressure
$\hat{\psi}^{el}(\mathbf{F}^e) = \frac{G}{2}\left[\mathbf{F}^e : \mathbf{F}^e - 3\right] + \frac{G}{\beta}\left[(\det\mathbf{F}^e)^{-\beta} - 1\right]$	Elastic energy
$\hat{\psi}^{ch}(\boldsymbol{\varphi}_R, \nabla\boldsymbol{\varphi}_R) = N_v k_B \vartheta\left(\sum_{\alpha=1}^{n}\varphi_R^\alpha \ln\varphi_R^\alpha\right)$	Chemical energy
$+ N_v \sum_{\alpha=1}^{n}\sum_{\beta=1}^{n}\Omega^{\alpha\beta}\varphi_R^\alpha\varphi_R^\beta$	
$+ \frac{1}{2}\sum_{\alpha=1}^{n}\sum_{\beta=1}^{n}\Gamma^{\alpha\beta}\,\nabla\varphi_R^\alpha \cdot \nabla\varphi_R^\beta$	

The system of equations presented in Table 1 describes the behavior of an elastic solid solution composed of n chemical components, where α denotes the α-th component and σ represents the reference species. The variables and parameters used in this model are listed in Table 2. Note that independent variables are indicated with [I]. A free-energy density $\psi_0 = 2N_v k_B \vartheta$ allows to write a cross-diffusion tensor as follows

$$\boldsymbol{D}^{\alpha\beta} = \psi_0 \boldsymbol{M}^{\alpha\beta}. \tag{3}$$

As suggested by Clavijo et al. [6, 7], the dimensionless forms of the energy densities, and governing and constitutive equations, can be obtained by

$$\overline{\mathbf{u}} = u_0^{-1}\mathbf{u}, \qquad \overline{\mathbf{x}} = L_0^{-1}\mathbf{x}, \qquad \overline{t} = D_0 l_0^2 L_0^{-4}t. \tag{4}$$

Further, the considered coupled chemo-mechanical theory uses the following scalar and vector dimensionless numbers

$$\omega^\alpha, \quad \overline{k}_+^c = k_+^c D_0^{-1}\ell_0^{-2}L_0^4, \quad \overline{k}_-^c = k_-^c D_0^{-1}\ell_0^{-2}L_0^4, \quad \overline{\vartheta}_c^{\alpha\beta} = \vartheta^{-1}\vartheta_c^{\alpha\beta},$$

$$\overline{\ell}^{\alpha\beta} = L_0^{-1}\ell^{\alpha\beta}, \quad \overline{\psi} = \hat{\psi}\psi_0^{-1}, \quad \overline{\sigma}^{\alpha\beta} = \sigma^{\alpha\beta}(\psi_0 L_0)^{-1}, \quad \beta, \quad \overline{\mathbf{b}} = G^{-1}\mathbf{b}, \tag{5}$$

$$\overline{G} = G\psi_0^{-1}, \quad l = u_0 L_0^{-1}, \quad \overline{\boldsymbol{D}}^{\alpha\beta} = \boldsymbol{D}^{\alpha\beta}D_0^{-1}\ell_0^{-2}L_0^2, \quad \overline{\gamma}^\alpha = \psi_0^{-1}\gamma^\alpha.$$

Table 3 presents a summary of the main dimensionless equations and variables in the chemo-mechanical framework, as outlined in the works of Clavijo et al. [6, 7]. When combined with equations 5, they constitute a complete system of partial chemo-mechanical equations that describes the system under study.

Table 2: List of variables and parameters of the coupled chemo-mechanical framework

Variables and Parameters	Description
N_v	Number of molecules per unit volume [I]
k_B	Boltzmann constant [I]
ϑ	Temperature [I]
ϑ_c	Critical temperature [I]
σ	Interfacial tension [I]
$\boldsymbol{M}$	Species mobility
ρ_0, ρ	Reference and current configuration solid densities
φ, φ_0	Species concentration, Initial species concentration [I]
J	Jacobian
$\boldsymbol{u}$	Displacement vector
$\mathbf{C}$	Green-Lagrange stress tensor
$\mathbf{F}$	Deformation gradient
$\mathbf{F}^e$	Elastic part of the deformation gradient
ψ	Chemo-mechanical free-energy density
γ	Internal micro-force
υ, ϖ	Stoichiometric coefficients in reversible reaction [I]
k^+, k^-	Reactions rates in reversible reaction [I]
L_0	Domain length [I]
$\boldsymbol{D}$	Diffusion tensor [I]
u_0	Reference deformation state [I]
D_0	Reference diffusion coefficient [I]
l_0	Interface thickness of a reference species [I]
t	Time
G	Shear modules [I]
β	Weak compressibility [I]
$\mathbf{b}$	Body force
ω	Chemical deformation parameter [I]
$\mathbf{T}_{\mathrm{R}}$	First Piola-Kirchhoff stress tensor

Table 3: Coupled system of dimensionless chemo-mechanical equations

Dimensionless Equation	Description
$\frac{\partial \varphi_{\mathrm{R}}^{\alpha}}{\partial \bar{t}} = \overline{\nabla} \cdot \left(\sum_{\beta=1}^{n} \overline{\boldsymbol{D}}^{\alpha\beta} \overline{\boldsymbol{M}} \ \overline{\nabla} \overline{\mu}_{\mathrm{R}\sigma}^{\beta} \right) + \overline{s}^{\alpha}$	Balance species concentrations
$\overline{\boldsymbol{M}} = \det(\mathbf{I} + l\overline{\nabla}\overline{\boldsymbol{u}})(\mathbf{I} + l\overline{\nabla}\overline{\boldsymbol{u}})^{-1}\mathbf{I}(\mathbf{I} + l\overline{\nabla}\overline{\boldsymbol{u}})^{-\top}$	Species Mobility
$\overline{\mu}_{\mathrm{R}\sigma}^{\alpha} = \frac{1}{2} \left(\ln \frac{\varphi_{\mathrm{R}}^{\alpha}}{\varphi_{\mathrm{R}}^{\sigma}} \right) + 2 \sum_{\beta=1}^{n} (\overline{\vartheta}_c^{\alpha\beta} - \overline{\vartheta}_c^{\alpha\beta}) \varphi_{\mathrm{R}}^{\beta} - \sum_{\beta=1}^{N} (\overline{\sigma}^{\alpha\beta} \overline{\ell}^{\alpha\beta} - \overline{\sigma}^{\sigma\beta} \overline{\ell}^{\sigma\beta}) \overline{\Delta} \varphi_{\mathrm{R}}^{\beta}$ $- \frac{1}{3} \omega^{\alpha\sigma} \mathrm{J}_{\varphi}^{-1} \overline{G} \mathrm{tr}[\overline{\mathbf{T}}_{\mathrm{R}}(\mathbf{I} + l\overline{\nabla}\overline{\boldsymbol{u}})^{\top}] - (\overline{\gamma}^{\alpha} + \overline{\gamma}^{\sigma})$	Species chemical potential
$\overline{s}^{\alpha} = -\sum_{c=1}^{n_s} \left\{ (\upsilon^{c\alpha} - \varpi^{c\alpha})(\overline{k}_+^c \prod_{a=1}^{n} (\varphi_{\mathrm{R}}^a)^{\upsilon^{ca}} - \overline{k}_-^c \prod_{a=1}^{n} (\varphi_{\mathrm{R}}^a)^{\varpi^{ca}}) \right\}$	Species Mobility
$\mathbf{0} = \mathrm{Div} \overline{\mathbf{T}}_{\mathrm{R}} + \overline{\mathbf{b}}$	Balance linear momentum
$\overline{\mathbf{T}}_{\mathrm{R}} = \mathrm{J}_{\varphi}^{-1/3}[\mathrm{J}_{\varphi}^{-\frac{1}{3}}(\mathbf{I} + l\overline{\nabla}\overline{\boldsymbol{u}}) - (\det \mathrm{J}_{\varphi}^{-\frac{1}{3}}(\mathbf{I} + l\overline{\nabla}\overline{\boldsymbol{u}})^{-\beta}(\mathrm{J}_{\varphi}^{-\frac{1}{3}}(\mathbf{I} + l\overline{\nabla}\overline{\boldsymbol{u}}))^{-\top}]$	First Piola-Kirchhoff stress tensor

3 A thermodynamically-consistent description of chemo-mechanical interactions in solid solutions

We encourage the reader to refer to the works of Clavijo et al. [5, 6, 7] for a detailed and comprehensive thermodynamic derivation of the coupled chemo-mechanical equations discussed in this manuscript. In this section, we aim to provide a deeper understanding of the underlying physics behind these equations and their connection to standard chemo-mechanical processes in geosystems. To begin, we introduce the solid model proposed by Larché-Cahn, which we use to illustrate the mechanism of interfacial interactions in a crystalline solid. By defining solidity, we can then explain the main components of the proposed free energy in Clavijo et al. [7], such as the elastic energy and chemical energy, and use them to estimate the thermodynamic pressure. Additionally, we provide observational evidence of such processes reported in the literature, further reinforcing the validity of our proposed framework. It's worth noting that our proposed framework is not only limited to metamorphic rocks but also to other natural phenomena that involve chemo-mechanical interactions.

3.1 Crystalline structure and mass constraint

The considered chemo-mechanical framework builds on the Larché-Cahn's solid model undertaking compositional changes [21, 22, 23, 20]. The author's model is based on the definition of relative chemical potentials following the so-called Larché-Cahn derivative [14, 21]. Hence, two different species may share the same lattice site in the crystalline structure due to energy exchange caused by species transport. For saturated systems, the chemical potential describes how the energy changes when one species increases its concentration while simultaneously reducing another one. Thereby, diffusion processes are only feasible if local composition variations of one species induce a complementary change in another species concentration.

Our formulation uses non-Fickian diffusion to describe interfacial interactions that describe, for example, spontaneous spinodal decomposition processes, the Ostwald ripening, and Gibbs-Thomson effects. However, the model describes conventional diffusion by setting the interfacial energy tensor equal to zero.

Understanding the impact of mechanical and chemical processes on solids requires a description of the nature of solidity and its properties. Gibbs' introduced a theory for the equilibrium thermodynamics of solids under non-hydrostatic conditions where dissolution and accretion at the solid-fluid interfaces are possible [13].

Gibbs' model describes non-hydrostatic stress distributions on solids caused by a surrounding fluid. This isotropic stress (pressure) induces fluid pressure gradients, ∇p^{fluid}, at solid-fluid interfaces, which in turn leads to chemical potential gradients at dissolution points. Nonetheless, Gibbs' theory does not quantify the lattice deformation caused by compositional changes as the solid-state diffusion concept did not exist [13, 36, 22]. We now model elastic solids that allow for compositional changes while remaining in the solid-state.
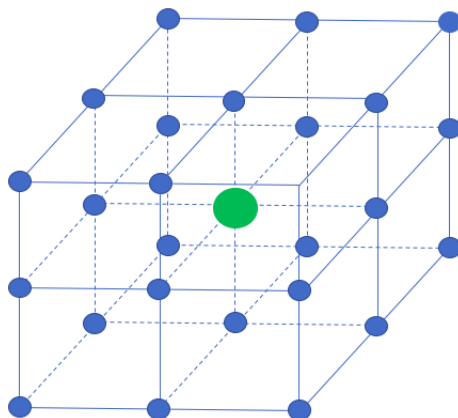
Figure 1: An idealized cubic crystalline structure. Atoms inside the crystalline structure are more energetically stable than surface ones since more neighboring atoms bound them.
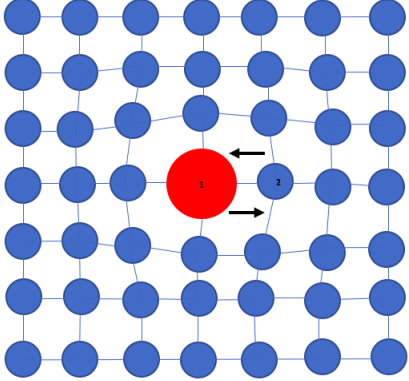
Figure 2: Larché and Cahn network embedded in a solid's crystalline structure. The solid is composed of two species sketched as red and blue circles. The figure shows a coherent transition together with the stress-assisted volume changes mechanism. The red atom transport from lattice site 1 to lattice site 2 induces volumetric stresses.

We adopt the network model proposed by Larché and Cahn [22]. Hence, a network embedded in the solid structure allows defining a displacement field and solid strains [14, 21]. As a result, the strain quantifies the network's deformation with respect to a reference network configuration, commonly set as an undeformed state. A solid network can be identified in several natural and engineering materials, such as minerals, polymers, and metals. For instance, the unit cell of the crystalline structure of minerals, which arranges the atoms in a systematic and repeating pattern, acts like a network. We focus on saturated systems, such that

$$\sum_{\alpha=1}^{n} \varphi^{\alpha} = 1, \tag{6}$$

where the order parameter φ_{α} accounts for the dimensionless concentration of the α-th species. When the solid is solely composed of the diffusing species, the mass constraint given by (6) must hold. Figure 2 depicts the crystalline structure composed of two species (drawn as red and blue circles) that corresponds to the case where adjacent components have coherent transitions, namely, their crystalline structure's orientation coincides. The solid network must account for the lattice misalignment when a new species grows and nucleates. According to Larché and Cahn [21, 22], Larche and Cahn [23, 20], the growth and nucleation of new species require describing non-coherent transitions by defining a crystalline structure and proper orientations of the mechanical properties. In our framework, the mass transport, nucleation, and growth of new species induced by chemical reactions generate elastic strains. In Figure 2, for instance, the transport of the red atom from the lattice site (1) to (2) must contribute to distorting the crystalline structure and, therefore, generating elastic strains. Henceforth, we denote such a mechanism as stress-assisted volume changes. The transport of the red atom from the lattice site (1) to (2) requires the movement of other atoms towards the lattice site (1) since the mass constraint is given by (6) must always hold. Thus, we restrict our attention to cases where mass transport by vacancies is impossible. In multicomponent systems, we also identify the partial pressure $p^{\alpha} = \varphi^{\alpha} p$ as the pressure related to the α-th species, with a concentration φ^{α}.

3.2   Interfacial interactions

Interfacial interactions explain Ostwald ripening effects. Such phenomena have been reported during the textural evolution of metamorphic rocks [29, 28, 11, 31]. This ripening effect is a thermodynamically-driven spontaneous process in spatially heterogeneous solutions composed of small and large aggregates. Thereby, the thermodynamic system moves to a lower energy state by minimizing its free-energy functional. Small aggregates tend to dissolve into the solution and precipitate onto the surface of larger aggregates of the same species since small aggregates are less energetically favored.

Without loss of generality, let us consider a solid solution with a cubic crystalline structure as depicted in Figure 1. The green atom is the most energetically stable in the crystalline structure due to its six
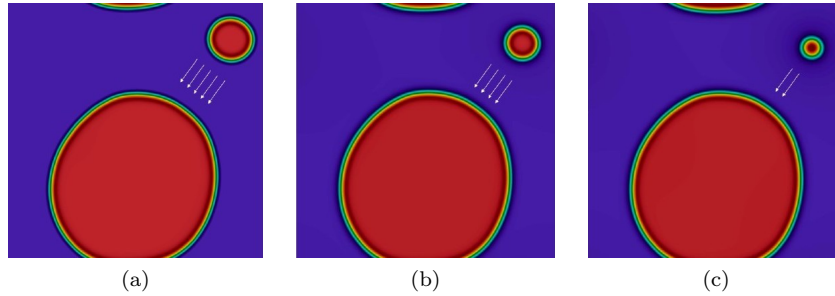
Figure 3: (a) Idealized solid composed of two aggregates and a matrix. Ostwald ripening dynamics control the dissolution of small aggregates and eventually their precipitation onto the surface of the larger aggregate once the solution supersaturates. (b) and (c)Sketch the ripening evolution. As the smaller inclusion concentration is depleted, the stress field changes, driving the large inclusion's final shape.

neighboring atoms. Meanwhile, the blue atoms on the surface are less energetically stable since five or fewer neighboring atoms bound them. The aggregates with more green (interior) atoms are energetically favored and, therefore, more stable. Consequently, as the system reduces its free-energy functional, the less stable structures, namely the smaller aggregates, tend to dissolve into the solution and precipitate on the surface of the more stable structures. This mechanism shrinks smaller aggregates and grows the larger ones, increasing the overall aggregate size. Figure 3 (a) shows an idealized representation of a rock composed of two aggregates and a matrix where the small aggregate of the red component undergoes Ostwald ripening. Eventually, the smaller red aggregate completely dissolves and precipitates, leading to the larger aggregate growth. Figure 3 (b)-(c) portrait intermediate stages of the process.

3.3 Elastic energy

Elastic energy defines the potential energy stored in the material as work is performed to change either its volume or distort its shape. External forces applied through solid boundaries, body forces due to gravity, electric and magnetic fields, thermal swelling/shrinkage, and internal adjustment caused by compositional changes transfer elastic energy to the solid.

The minerals that compose rocks accommodate these processes along with their evolution. Shear zones and overburden are typical examples of external loading applied to the rock. The chemical interactions caused by diffusion and reaction, where atoms arrange to form a material with a defined crystal structure, are examples of internal adjustment caused by compositional changes. Exhumation of deep crustal metamorphic rocks involves thermal swelling and shrinkage due to the crust's temperature gradient.

All elastic responses allow the solid to recover its original configuration when the external force ceases. Consequently, the solid recovers its shape and volume. More importantly, chemical systems under heterogeneous elastic stresses can only reach equilibrium if all dissipative processes, such as mass transport, chemical reactions, and interfacial effects, have ceased. In the considered framework, the variations in local species concentration are scaled by a swelling parameter ω, which measures the change in local species concentrations towards volumetric stresses. The parameter ω is related to the solid crystalline structure and its mechanical properties [6].

Figure 4 depicts the elastic energy $\hat{\psi}^{el}$ as a function of local species concentration, parametrized by the swelling parameter ω, for a two-component system. With fixed boundaries, the stress variations are only due to the changes in the species concentration. As illustrated in Figure 4, the elastic energy increases as the swelling parameter becomes larger. Thereby, as long as local species concentrations change with respect to the initial distribution, the solid undergoes elastic deformation. The interaction between diffusion and deformation changes the rates of both processes.
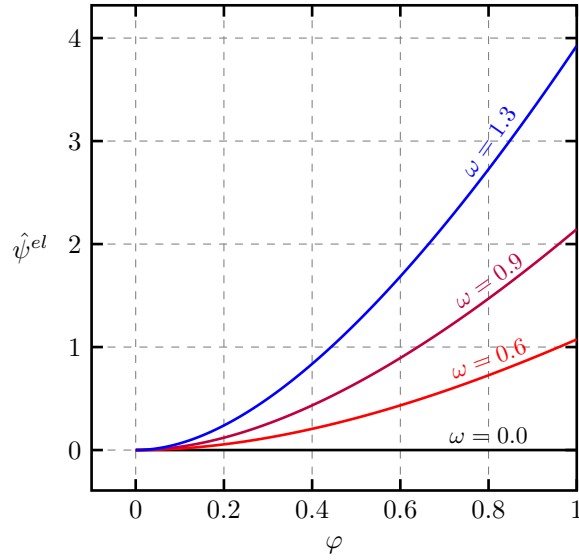
Figure 4: Elastic energy $\hat{\psi}^{el}$ as a function of the local concentration. The parametrization shows the effect of the swelling parameter ω on the elastic energy $\hat{\psi}^e$.
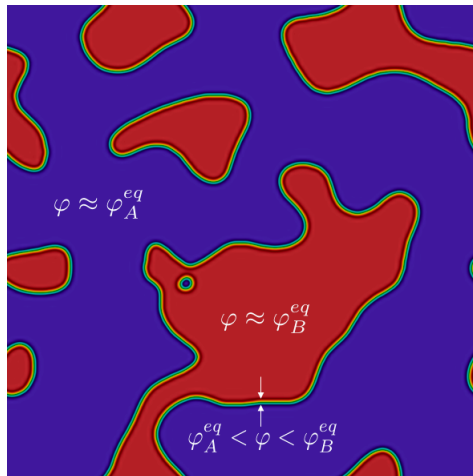
Figure 5: Solid solution microstructure composed of two components. The concentration of the components A and B correspond to φ_A^{eq} and φ_B^{eq}, respectively. The interface, where the concentration varies between φ_A^{eq} and φ_B^{eq}, embraces the chemical properties of both the components A and B.
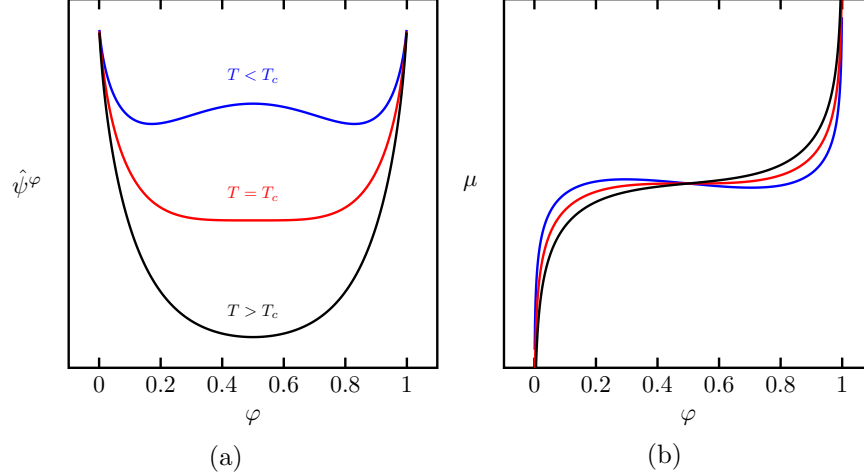
Figure 6: (a) represents the free energy potential of the homogeneous system. The double-well potential allows for the spinodal decomposition where the local minima of each well account for each component's equilibrium concentration. (b) sketches the chemical potential as a function of the concentration. By definition, the chemical potential is the free energy potential's partial derivative with respect to the local concentration.

3.4 Chemical energy

Solid solutions are complex systems composed of several chemical components. The interface between components may be of non-zero thickness where the physical and chemical properties vary from one component to another. That is, the transition from one component to another may not be sharp.

Figure 5 shows an idealized representation of two components A and B, in equilibrium, sketched by colors blue and red, respectively. The concentrations φ of A and B corresponds to φ_A^{eq} and φ_B^{eq}. Further, there exists a thin region (color gradient) where the concentration φ varies gradually between φ_A^{eq} and φ_B^{eq}. This region is the interface between components A and B.

If the temperature decreases below the system's critical temperature, spontaneous phase separation processes such as spinodal decomposition control the textural evolution in the material [6]. As a consequence, the system favors the formation of spatial domains rich in each component. Spinodal decomposition processes can occur, for example, in plagioclase feldspars and binary systems such as magnetite-ulvospinel [4, 24, 10].

The generalized Cahn-Hilliard equation can track the microstructure evolution of solid solutions. Figure 6 (a) depicts the homogeneous free-energy density $\hat{\psi}^\varphi$ as a function of the local concentration φ for different values of absolute temperature T. This potential corresponds to the case of a two components solid solution, for instance, A and B as depicted in Figure 5. For absolute temperature values greater than critical ones (i.e., $T > T_c$), the potential $\hat{\psi}^\varphi$ becomes a convex-downward function of φ. The latter renders a homogeneous mix, as it only exits a single stable state located at the minimum value of $\hat{\psi}^\varphi$. Hence, for all possible values of concentration, the free-energy density is stable. Alternatively, when the absolute temperatures are below the critical temperature $T < T_c$, the homogeneous free-energy functional becomes a double-well convex upward function. As a consequence, two stable coexistent components emerge from each local minimum value, representing the concentration at equilibrium. Figure 6 (b), on the other hand, showcases the chemical potential calculated as the derivative of the homogeneous, free-energy functional $\hat{\psi}^\varphi$ with respect to the local concentration φ.

3.5 Helmholtz free-energy density and the thermodynamic pressure

The Helmholtz free-energy density results from applying the Legendre transform to the internal energy while replacing the system's entropy by the temperate as an independent variable. Moreover, by subordinating the constitutive relationships to the Helmholtz free-energy density following the arguments of Noll et al. [32], this framework describes the dynamics of a non-linear elastic solid undergoing chemical processes and

deformation. The thermodynamic pressure is then estimated as the partial derivative of the Helmholtz free-energy density with respect to the specific volume, while keeping local concentrations and deformation constant. This physical quantity defines the chemical equilibrium when all dissipative processes, which produce entropy and therefore variations in local composition, cease [16, 13].

3.6 A review of thermodynamic pressure in geosystems

A spike of recent interest in the geosciences literature is the proper definition of the thermodynamic equilibrium in metamorphic systems. As outlined in Section 1, the thermodynamic pressure can have spatio-temporal inhomogeneities.

Recent studies of metamorphic petrology show localized pressure deviations from lithostatic values, arising from complex chemo-mechanical interactions between the minerals. Conventionally, pressure is estimated as the Archimedes' value (directly proportional to the depth). When considering deforming rocks and mineral reactions, stress emerges from both volume changes due to chemical reactions and the overburden, leading to inhomogeneous pressure distributions. Thus, Archimedes's formula is inaccurate for these systems when considering volume changes arising from chemical processes. Nonetheless, the magnitude of such deviations is still under debate. However, heterogeneity is likely to be the result of the composition of volume changes due to chemical reaction and residual stresses due to solidification and plastification.

For instance, the formation of ultrahigh-pressure rocks suggests that pressure does not always translate into depth [30]. Understanding the nature of such deviations is crucial since pressure provides a constraint for the description of the dynamics of orogens and an indirect measurement of the depth history of the sample. The roots of such discrepancies are complex chemo-mechanical interactions as the metamorphic rock complexes evolve towards equilibrium, Most importantly, chemo-mechanical responses are strongly interdependent.

Moulas et al. [30] provide a comprehensive review on metamorphic rocks maintaining and recording significant pressure deviations from the lithostatic values. During prograde metamorphism, high pressure and temperature conditions form garnet porphyroblasts. As quartz and coesite inclusions grow, the metamorphic system endures large volumetric stresses associated with expanding inclusions in a relaxed host matrix. Eventually, the metamorphic system exhibits chemical zonation where each aggregate has different chemical and mechanical properties. Such heterogeneity generates spatial variations in pressure.

The effect of inhomogeneous pressure distributions seem to be critical. Therefore, understanding the nature of such natural responses will allow the geoscience community to calibrate geodynamics models and to describe the evolution of microstructure. Previous studies of metamorphic rocks separated the chemical and the mechanical actions on mineral assemblages. Given the previous discussion, this simplifying splitting is inappropriate as volume changes, induced by chemical interactions between minerals, strongly influence pressure distribution. Thus, an appropriate description of the deformation process requires a comprehensive treatment of the coupled chemo-mechanical process.

4 Modeling the effects of inhomogeneous pressure distributions in a ternary solid solution

In this section, we explore deformation resulting from chemical processes, i.e, mass transport, interfacial effects, and chemical reaction. We use the thermodynamic pressure of the system to showcase the impact of chemical processes.

We model the dynamics of a ternary solid and treat the system as a general multicomponent solid whose crystalline structure imposes a mass constraint such that (6) holds. One of the components emerges from a forward chemical reaction. The chemical reaction occurs in solid-state, and as it proceeds, the new component grows and nucleates. As mentioned above, we do not consider either diffusion by vacancies or grain boundaries between the components. In other words, the crystalline structure of each component, described by a lattice such as Figure 2, is coherent. We portray the scenario where local volume changes caused by chemical interactions trigger the stress generation in the solid, reflecting spatial variations in pressure. This physical quantity corresponds to the thermodynamic pressure described in Section 3.5. We
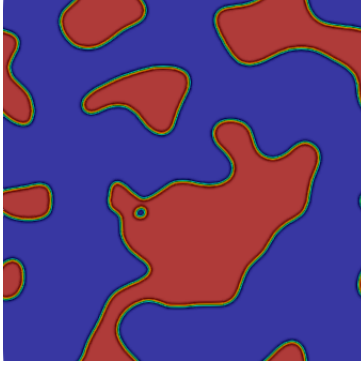
Figure 7: An sketch of the initial concentrations for A and B. Regions colored by red and blue represent A and B, respectively. As the chemical and mechanical processes evolve, the system favors generating a new component C, contributing to the volumetric stress formation in the solid as C nucleates and grows.

use the diffusion coefficients, the reaction rates, and the thermodynamic properties commonly found in mineral solid solutions. Table 4 covers such quantities. The overall reaction is given by

$$A + B \xrightarrow{k} C. \tag{7}$$

Moreover, $\varphi_1 = [A]$, $\varphi_2 = [B]$ and, $\varphi_3 = [C]$ define the concentration of the components A, B and C, respectively. We solve the system of equations using PetIGA [9], with a square domain $\Omega = [0,1]^2$ with 128 C^1-quadratic finite elements. To avoid spurious numerical instabilities due to time discretazation, we use the generalized-α method proposed in Sarmiento et al. [35].

Figure 7 depicts the spatial distribution of species initial concentrations. The initial concentration of C is zero. We also assume a solid without distortions at $\bar{t} = 0.0$. This implies zero relative displacements in the sample and, thus, zero strains. We choose a spatial distribution of the concentrations, as Figure 7 shows, to account for large concentration gradients to track the effect of the interface evolution [3], namely, the contribution of the curvature in the chemical potential. We are interested in observing the effect of local variations in the concentration upon the generation of inhomogeneous stress and pressure distributions which relate the concentrations to the deformation gradient as captured by a volumetric stress tensor. Hence, the stress variations come from the volumetric deformation since we do not impose external loading nor deformation. Furthermore, there are no mass fluxes through the boundaries. Following Gurtin et al. [14], the deformation itself cannot induce mass transport. Therefore, for mass transport to happen, there must be chemical potential gradients where the chemo-mechanical coupling accounts for the contributions from both the solid's physical and chemical responses, which in the material sciences literature is known as the absence of a piezo-diffusive effect. We set the chemical energy parameter and the number of molecules per volume so that we guarantee a non-convex triple-well energy functional. For instance, Figure 6 models a two-component case. If required, one can set the chemical energy such that the system evolves without interfacial interactions.

Figures 8-11 show the temporal evolution of the concentration of component A, B, and C together with the spatial distribution of the thermodynamic pressure, p^{th}, as the solid evolves to equilibrium. Unlike the thermodynamic pressure, the concentrations and time evolution are dimensionless quantities. As discussed above, we calculate the concentration of C, φ_3, by applying at each time-step the constraint defined by (6), which guarantees the consistency of the process. At early stages $\bar{t} < 5.6\text{x}10^{-4}$, Figure 8, the non-Fickian diffusion essentially controls the temporal evolution of both the physical and mechanical processes as the forward chemical reaction plays no substantial role. One can verify such assertion by checking the mass evolution in Figure 12, where during $\bar{t} < 2.63\text{x}10^{-3}$ the masses remain approximately constant. Moreover, from Figure 8, one can also infer that there is no formation of C until $\bar{t} > 5.6\text{x}10^{-4}$. Therefore, the initial condition, spatially distributed as Figure 7, goes through spinodal decomposition during the early stages and is followed by coarsening [5]. These interactions lead to a merging process which eventually forms large and rounded structures as suggested by Figures 8 and 9. Hence, we conclude that variations in local composition caused by diffusion define the stress generation source at the early stages. Therefore, the dynamics of the

12

spatially inhomogeneous pressure distribution results solely from both spinodal decomposition and coarsening mechanisms. At the same time, the system minimizes its free-energy functional by reducing the interface between the components A, B, and C. Figure 12 also depicts the temporal evolution of the interfacial energy, which verifies that during $\bar{t} < 2.63\mathrm{x}10^{-3}$, in particular for A and B, the interfacial energy decreases. Furthermore, the stress-assisted volume changes mechanism primally occurs along the boundary between A and B as the system forms the rounded structures. Namely, large stresses arise along the interface between A and B. Figure 14 reports the dynamics of the neo-Hookean energy functional which captures the shrinkage and swelling process as the components diffuse and react through the solid structure. From the free-energy functional evolution, Figure 13, shows that the system is minimizing its free-energy functional as the dissipative diffusion process occurs. The minimization is a direct consequence of the minimum energy principle, which states the internal energy is minimized as the system reaches constant entropy. The free-energy functional describes the contribution from both the physical and chemical responses of the solid. As discussed in Section 3.4, the model captures the dynamics of the Ostwald ripening [28, 11, 31]. In the range between $1.73\mathrm{x}10^{-3} < \bar{t} < 2.63\mathrm{x}10^{-3}$, Figure 9 illustrates that the smaller aggregates of component A tend to dissolve into the solid solution and precipitate along the surface of the larger aggregates. Such mechanism leads to a large rounded structure of A which is entirely enclosed by B. Figure 9 also shows the heterogeneous distribution of the thermodynamic pressure. The thickness of the reaction layer between A and B is irregular; see Figure 9 (c)-(d). Conventionally, during reaction-diffusion processes, one can expect a planar growth of the reaction layer. Nevertheless, when considering reaction-induced stresses and interfacial contributions, the chemical potential becomes a function of both the surface curvature and the mechanical pressure, leading to an irregular reaction layer of thickness. As a result, the diffusion process's driving force changes along with the reaction layer, which induces different diffusion rates at the reaction boundary. The forward chemical reaction occurs mainly during the time interval between $8.02\mathrm{x}10^{-3} < \bar{t} < 3.91\mathrm{x}10^{-2}$, see Figure 10. Milke et al. [27] define that positive volume changes involve space creation by moving out the mass from the reaction site, and thus, the reaction products can grow and accommodate. On the contrary, negative volume changes induce mass transport into the reaction site by consuming the reactant components. During this stage, the system forms C along the boundary between A and B.

Experimental evidence of reaction rim growth is reported by Milke et al. [26] whose experiments on the system forstatite (fo) - quartz (qtz) - enstatite (en) produce a reaction rim, mainly composed of enstatite (en), of irregular thickness. They suggest that this behavior's nature is due to the mechanical contributions to the chemical potentials resulting from the local volume changes caused by the reaction. Although the mechanical contributions influence the chemical potentials, one must also consider the contributions of surface curvature between the components. They also alter to a large degree the chemical potentials. This curvature effect is called the Gibbs-Thomson effect [33, 18, 1]. The rim growth mechanism as defined by metamorphic petrologists results from the chemical reaction between neighboring minerals [27, 19]. In particular, this process is strongly affected by the solid's mechanical properties and involves large volume changes that lead to large isotropic stresses.

Eventually, the volumetric stress drives the spatial variations in pressure. Moreover, one can verify from Figure 12 that in the range between $8.02\mathrm{x}10^{-3} < \bar{t} < 3.91\mathrm{x}10^{-2}$ the masses change as well as the interfacial energy. Consequently, the reactant A and B masses tend to decrease while the reaction product C increases. At the end of such stage, the system completely consumes the mass of A. As expected, the interfacial energy of C increases as the forward reaction generates more C. Following Clavijo et al. [5], the reaction term in the chemical process increases the free-energy functional of the system resulting in the growth trend depicted by Figure 13 in the interval $8.02\mathrm{x}10^{-3} < \bar{t} < 3.91\mathrm{x}10^{-2}$. Finally, the interleaving between the chemical and mechanical responses of the solid form an elongated structure along the solid primally composed of B and surrounded by C.

Due to large volume changes associated with the chemical process, we can see the stresses in the solid and thereby the notorious inhomogeneous pressure distribution at the steady-state. Figure 13 shows that from $\bar{t} > 7.99\mathrm{x}10^{-2}$ all dissipative processes ceased as the free-energy functional remains constant. Hence, the pressure strongly depends on the interactions between the physical and chemical responses of the solid. It is worth noticing that the resulting variations in pressure cannot be compared against deviations from lithostatic values as we do not consider in situ stresses.

The red dots show in Figure 13 represent the beginning of the processes mentioned above. In particular, one and two accounts for the beginning of the spinodal decomposition and coarsening processes, respectively.

13

Table 4: Physical and Chemical parameters

Physical parameter	Value	Name
ϑ [K]	1373.15	Temperature
ϑ^c [K]	1500.0	Critical temperature
D [m^{2}s^{-1}]	10^{-20}	Diffusion coefficient
K^+ [m^{2}s^{-1}]	10^{-14}	Reaction rate
σ [J m^{-2}]	0.817	Interfacial energy
ℓ [m]	10^{-8}	Interface thickness
μ [GPa]	44	Shear modulus
ν [-]	0.17	Poisson's ratio
ω [-]	10^{-2}	Swelling parameter

Analogously, between three and four, the system undergoes ripening. Finally, five and six define the forward chemical reaction period and the steady-state of the solid, respectively.

The possibility of describing the formation of metamorphic mineral aggregates with spatial inhomogeneous pressure distributions collides with the classical description of metamorphic minerals' formation. The classical interpretations assume an isotropic thermodynamic equilibrium to explain metamorphic mineral assemblages via thermobarometry techniques and phase diagrams. Therefore, the formation processes that induce heterogeneous pressure distributions imply that these techniques may not be robust to characterize metamorphic systems. That is, these inhomogeneous pressure conditions contradict the foundational assumptions of uniform pressure and temperature distributions. Thus, the nature of the pressure distribution that defines the equilibrium of metamorphic rocks and how to calculate and determine this quantity are still open questions. As pointed out by Hobbs and Ord [15] (and references therein), the thermodynamic equilibrium is entirely characterized by the thermodynamic pressure given by the partial derivative of the Helmholtz free-energy density with respect to the specific volume, or when considering Gibbs free-energy density, the partial derivative has to be taken with respect to the volume. We believe that previously, in the geosciences literature, the lithostatic pressure has erroneously been used to describe the state of equilibrium of the metamorphic rocks. And recently, works on inhomogeneous pressure distributions use the mean stress to characterize equilibrium conditions [38, 37]. These pressure definitions only make sense, from a thermodynamic point of view, for elastic solid in the absence of ongoing chemical processes [15].

Viscoelastic, plastic, diffusional creep responses and ongoing chemical processes lead to additional contributions to thermodynamic pressure. Hobbs and Ord [15, 16] have carried out an extensive review on the subject (see also e.g Bennethum and Weinstein [2] and references therein).
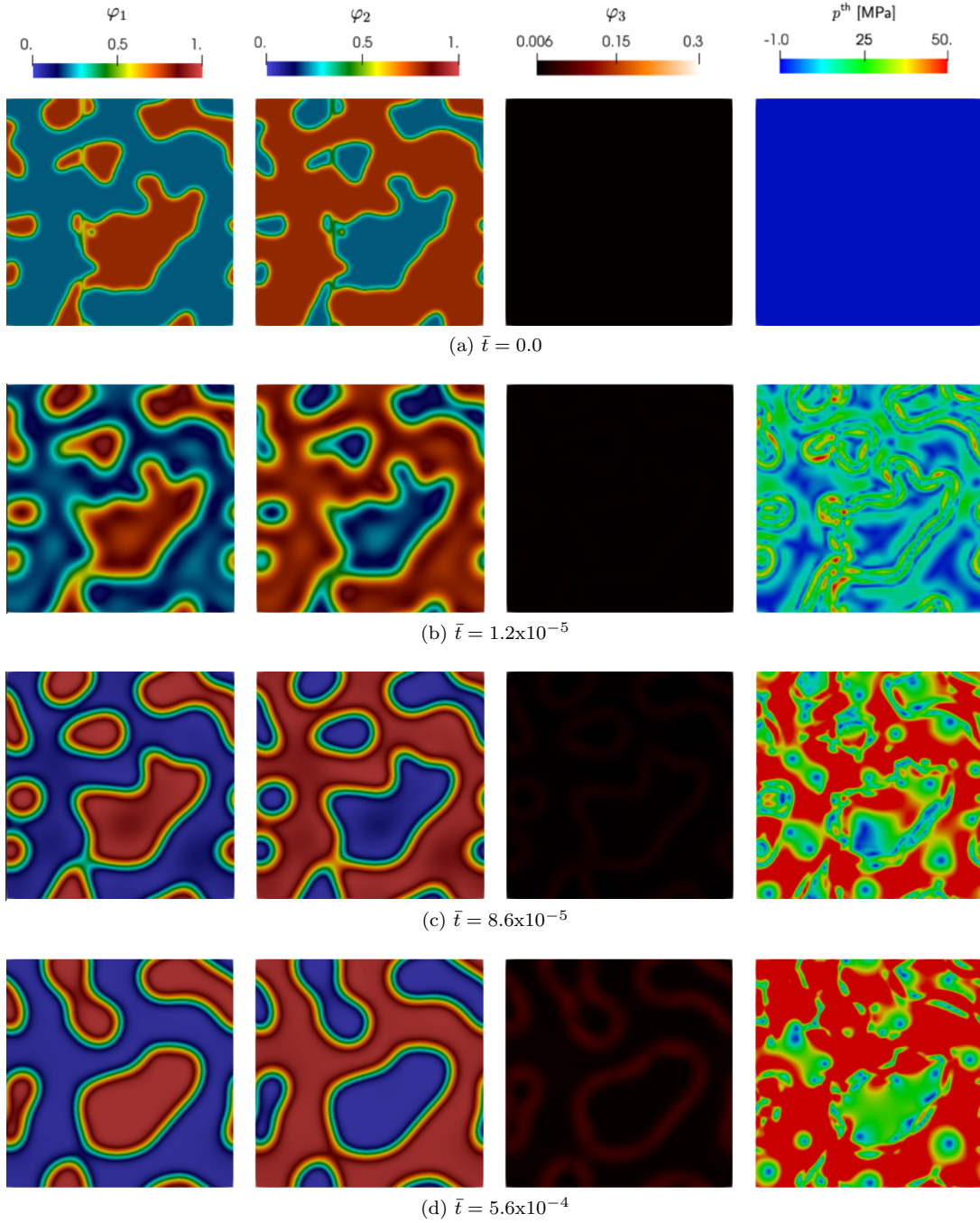
Figure 8: Behavior of the ternary solid at the early stages $\bar{t} \leq 5.6\text{x}10^{-4}$. The system is mostly controlled by spinodal decomposition and coarsening. Thereby, the volume changes and concomitant stress generation result from the diffusion process, leading to the inhomogeneous pressure distribution.

15

(a) $\bar{t} = 1.73\mathrm{x}10^{-3}$

(b) $\bar{t} = 1.9\mathrm{x}10^{-3}$

(c) $\bar{t} = 2.5\mathrm{x}10^{-3}$

(d) $\bar{t} = 2.63\mathrm{x}10^{-3}$
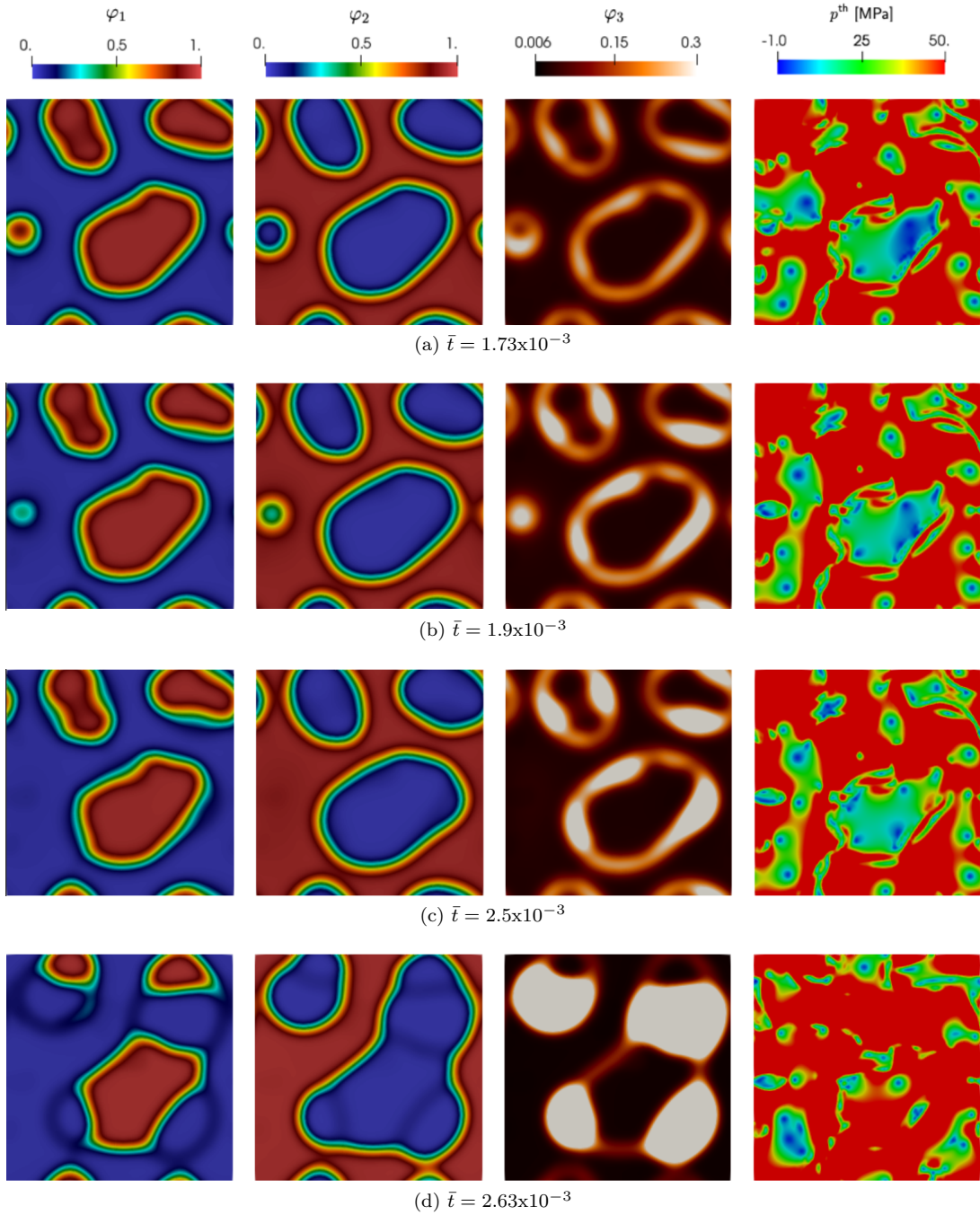
Figure 9: Dynamics of the system following Ostwald ripening. Unstable particles on the surface dissolve and go into the solution. As the solution gets supersaturated, particles tend to precipitate onto the surface of the more stable structures. Consequently, the larger structures grow.

(a) $\bar{t} = 8.02 \text{x} 10^{-3}$

(b) $\bar{t} = 9.5 \text{x} 10^{-3}$

(c) $\bar{t} = 1.76 \text{x} 10^{-2}$

(d) $\bar{t} = 3.91 \text{x} 10^{-2}$
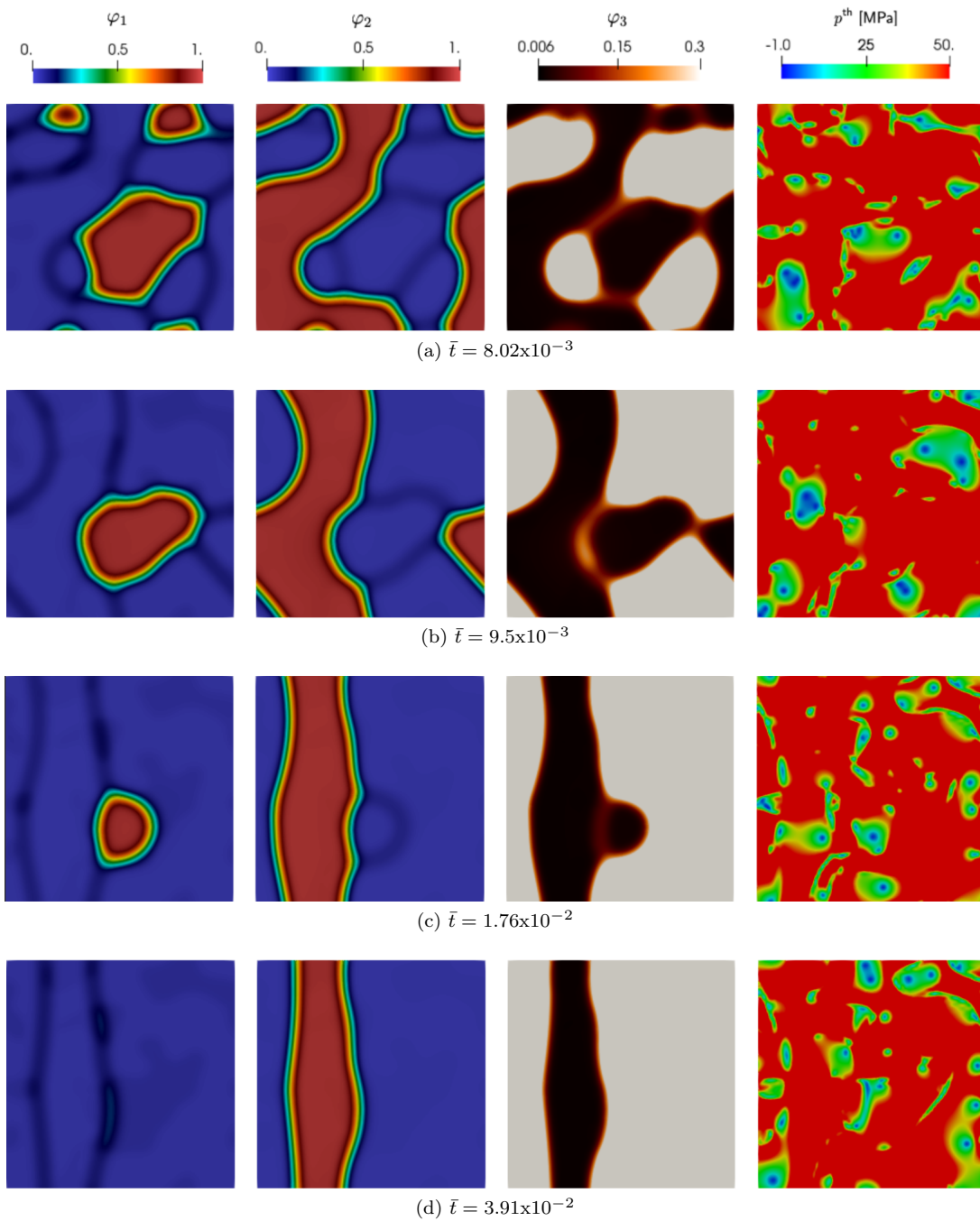
Figure 10: Reaction between the components A and B produces a new component C along their boundary. The evolution favors consuming in a more significant proportion A than B. The simulation results show how nucleation and growth induce volumetric stresses, contributing to generating the inhomogeneous pressure distribution.

(a) $\bar{t} = 3.54 \text{x} 10^3$

(b) $\bar{t} = 9.33 \text{x} 10^4$

(c) $\bar{t} = 1.0 \text{x} 10^5$

(d) $\bar{t} > 1.0 \text{x} 10^5$
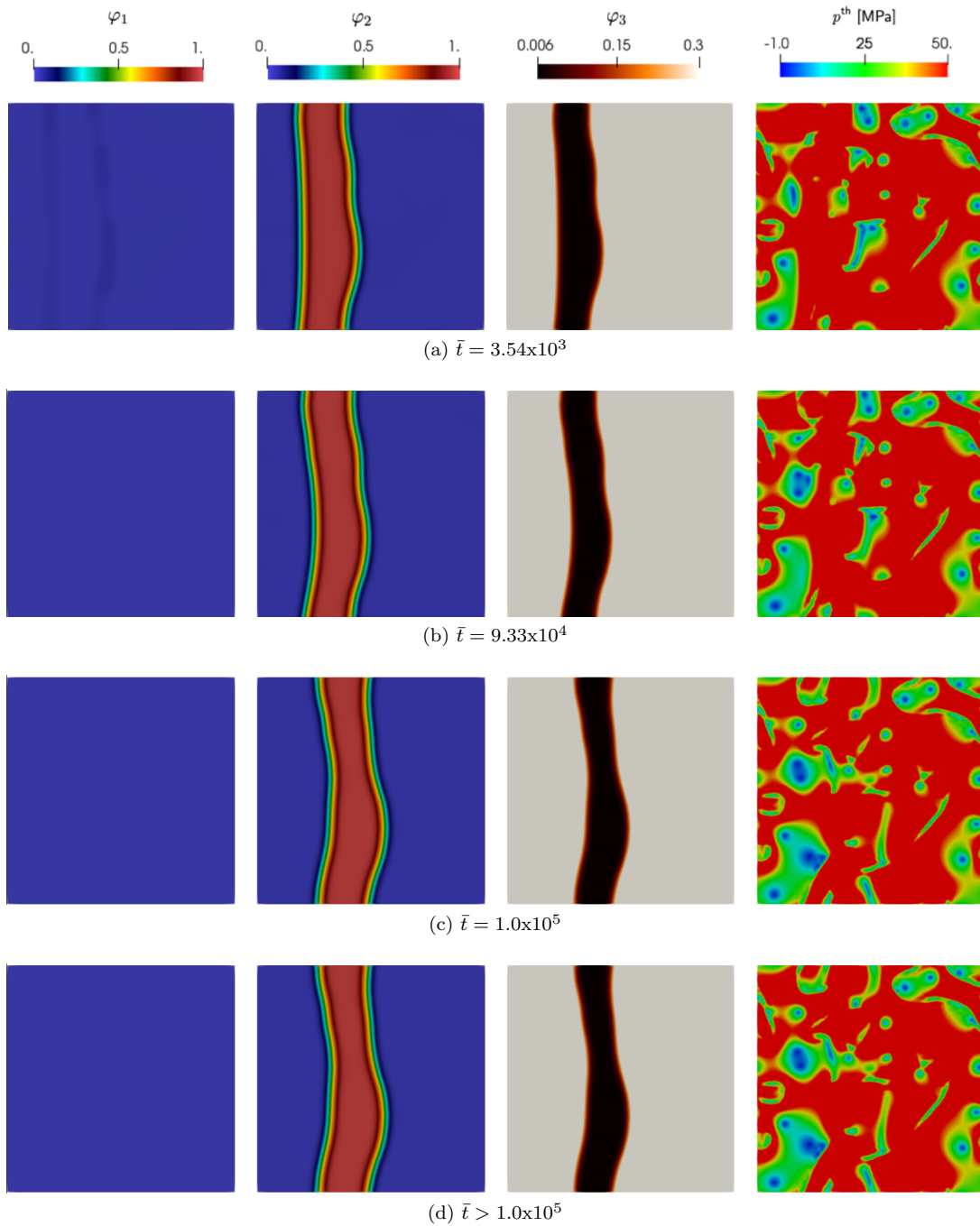
Figure 11: The chemical reaction ceases at $\bar{t} = 9.33 \text{x} 10^4$, Figure (b). From this point on, the system minimizes its free energy solely through mass transport, resulting in a steady state at $\bar{t} > 9.33 \text{x} 10^6$. The equilibrium of the solid solution is ultimately determined by the thermodynamic pressure at $\bar{t} > 9.33 \text{x} 10^4$, which takes into account both the chemical and mechanical responses of the solid.
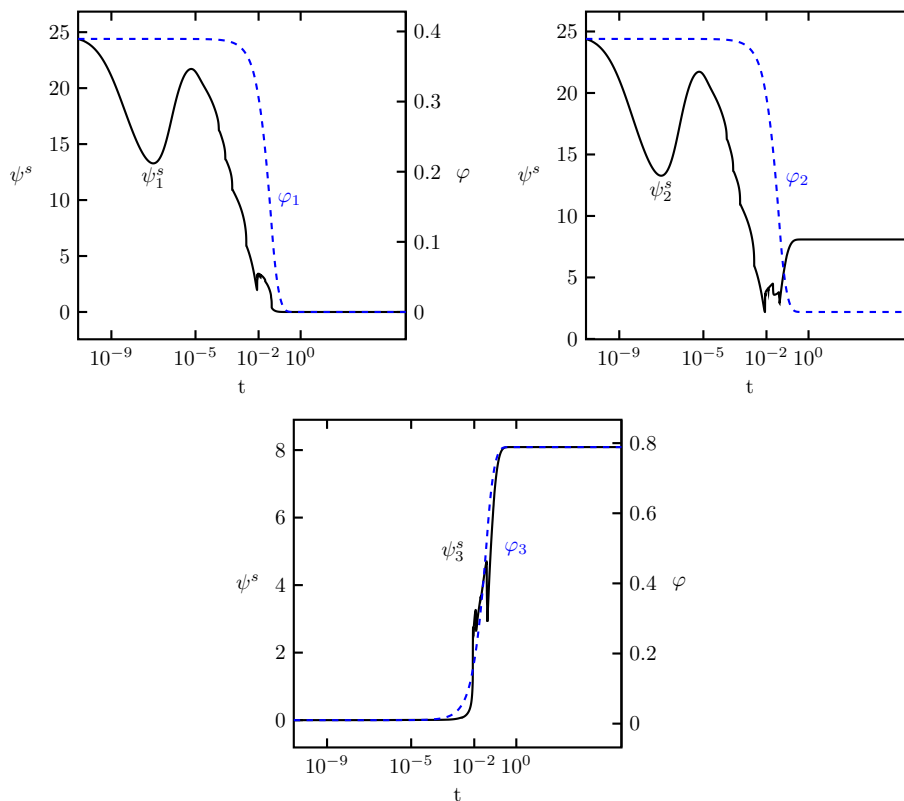
Figure 12: When a system undergoes a chemical process, either mass transport or chemical reaction, the dynamics favors to either produce or destroy the interface between the species changing the interfacial energy.
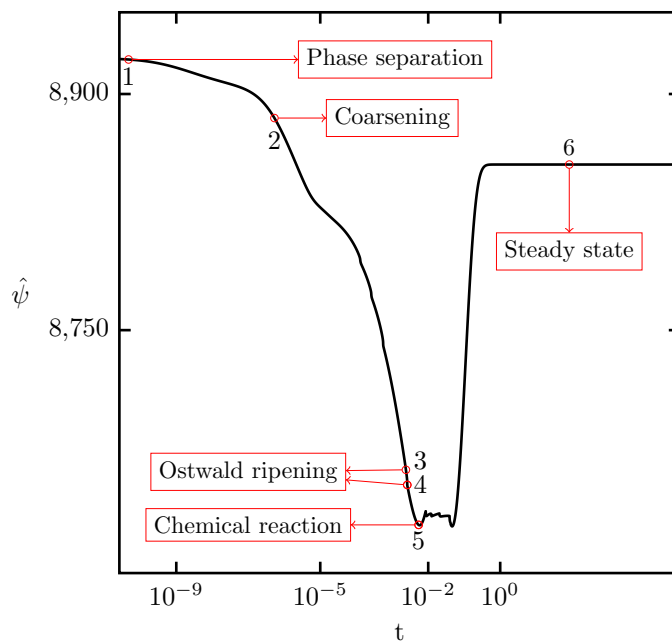
Figure 13: Free-energy functional evolution and beginning of processes such as spinodal decomposition and coarsening, Ostwald ripening effect, the chemical reaction, and steady-state.

19
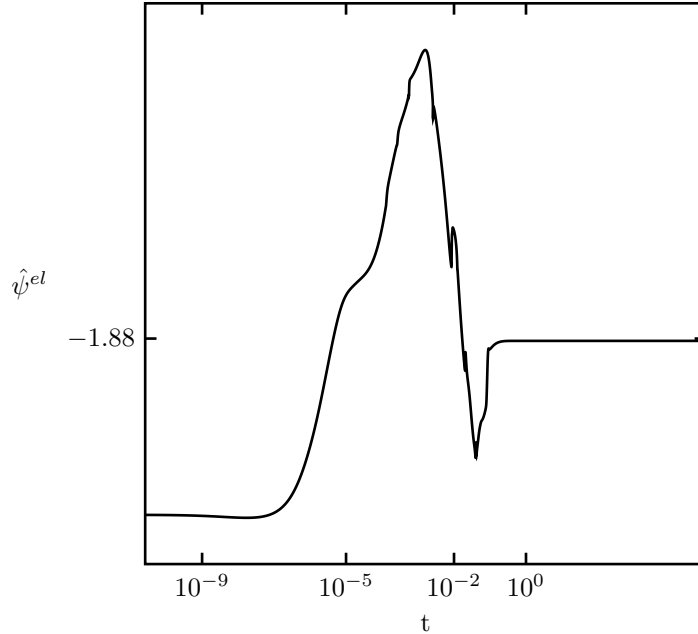
Figure 14: Elastic energy of a neo-Hookean solid model. Since no deformation is induced across the solid boundaries, the elastic energy variation entirely results from the volumetric stresses associated with the variations in local composition.

5   Conclusions

We portray how deformation affects a chemically active solid's evolution through continuum mechanics, thermodynamics far from equilibrium, and the phase-field model. This framework differs from previously published works extensively since the thermodynamic pressure, essentially to define equilibrium conditions in geosystems, is calculated from a fully coupled-thermodynamic framework for solid solutions. Furthermore, the framework accounts for multiple chemical components and interfacial effects. We include interfacial effects in the system thermodynamics because such interactions have been reported in the geoscience literature.

We demonstrate that the interleaving between chemical and mechanical interactions triggers spatial variations in pressure. The latter is still an open research topic in geoscience. Such a pressure corresponds to the thermodynamic pressure and defines the system's equilibrium conditions when it reaches a steady state. Hence, as mentioned earlier, the framework serves as a first step to modeling the behavior of stress-generation processes in mineral solid solutions. Nevertheless, one must be aware that spinodal decomposition mechanisms are not common processes in mineral solid solutions. Therefore, to model systems without interfacial contributions, the chemical energy must be set so that no spinodal decomposition occurs along the process. This can be achieved by choosing the initial distribution of the concentrations at the minimum values of the chemical energy and by setting to zero the interfacial energy tensor. The system does not tend to minimize the energy by spontaneous separation responses. As Section 4 discusses, the stresses arising from chemical processes such as mass transport and chemical reactions greatly influence the thermodynamic pressure values.

Figures 11 and 13 verify that the thermodynamic pressure can have inhomogeneous spatial distributions at steady state. Without loss of generality, we show that by selecting appropriate material parameters, one can capture common processes in geosystem. For instance, the geometry of reaction rim growth as reported by Milke et al. [26]. Herein, we do not include grain boundaries nor fluid-solid interactions. As mentioned above, this is necessary, for instance, when modeling metamorphism.

20

Acknowledgement

References

[1] F. Almgren and L. Wang. Mathematical existence of crystal growth with gibbs-thomson curvature effects. *The Journal of Geometric Analysis*, 10(1):1–100, 2000.

[2] L. S. Bennethum and T. Weinstein. Three pressures in porous media. *Transport in Porous Media*, 54 (1):1–34, 2004.

[3] J. W. Cahn and J. E. Hilliard. Free energy of a nonuniform system. i. interfacial free energy. *The Journal of chemical physics*, 28(2):258–267, 1958.

[4] M. A. Carpenter. A "conditional spinodal" within the peristerite miscibility gap of plagioclase feldspars. *American Mineralogist*, 66(5-6):553–560, 1981.

[5] S. Clavijo, A. Sarmiento, L. Espath, L. Dalcin, A. M. Cortes, and V. M. Calo. Reactive n-species cahn–hilliard system: A thermodynamically-consistent model for reversible chemical reactions. *Journal of Computational and Applied Mathematics*, 350:143–154, 2019.

[6] S. P. Clavijo, L. Espath, and V. M. Calo. Extended larché–cahn framework for reactive cahn–hilliard multicomponent systems. *Continuum Mechanics and Thermodynamics*, 33(6):2391–2410, 2021.

[7] S. P. Clavijo, L. Espath, A. Sarmiento, and V. M. Calo. A continuum theory for mineral solid solutions undergoing chemo-mechanical processes. *Continuum Mechanics and Thermodynamics*, 34(1):17–38, 2022.

[8] H. Dal and C. Miehe. Computational electro-chemo-mechanics of lithium-ion battery electrodes at finite strains. *Computational Mechanics*, 55(2):303–325, 2015.

[9] L. Dalcin, N. Collier, P. Vignal, A. Côrtes, and V. M. Calo. Petiga: A framework for high-performance isogeometric analysis. *Computer Methods in Applied Mechanics and Engineering*, 308:151–181, 2016.

[10] T. C. Droubay, C. I. Pearce, E. S. Ilton, M. H. Engelhard, W. Jiang, S. M. Heald, E. Arenholz, V. Shutthanandan, and K. M. Rosso. Epitaxial fe 3- x ti x o 4 films from magnetite to ulvöspinel by pulsed laser deposition. *Physical Review B*, 84(12):125443, 2011.

[11] D. D. Eberl, J. Środoń, M. Kralik, B. E. Taylor, and Z. E. Peterman. Ostwald ripening of clays and metamorphic minerals. *Science*, 248(4954):474–477, 1990.

[12] C. M. Elliott and H. Garcke. Diffusional phase transitions in multicomponent systems with a concentration dependent mobility matrix. *Physica D: Nonlinear Phenomena*, 109(3-4):242–256, 1997.

[13] J. W. Gibbs. On the equilibrium of heterogeneous substances. *American journal of science*, 3(96): 441–458, 1878.

[14] M. E. Gurtin, E. Fried, and L. Anand. *The mechanics and thermodynamics of continua.* Cambridge University Press, 2010.

[15] B. E. Hobbs and A. Ord. Does non-hydrostatic stress influence the equilibrium of metamorphic reactions? *Earth-Science Reviews*, 163:190–233, 2016.

[16] B. E. Hobbs and A. Ord. Coupling of fluid flow to permeability development in mid-to upper crustal environments: a tale of three pressures. *Geological Society, London, Special Publications*, 453(1):81–120, 2018.

[17] D. Howell, I. Wood, D. Dobson, A. Jones, L. Nasdala, and J. Harris. Quantifying strain birefringence halos around inclusions in diamond. *Contributions to Mineralogy and Petrology*, 160(5):705–717, 2010.

[18] C. A. Johnson. Generalization of the gibbs-thomson equation. *Surface Science*, 3(5):429–444, 1965.

[19] L. Keller. Mineral growth in metamorphic rocks: relationships between chemical patterns, mineral microstructure and reaction kinetics. In *AGU Fall Meeting Abstracts*, volume 2008, pages MR14A–04, 2008.

[20] F. Larche and J. Cahn. Thermochemical equilibrium of multiphase solids under stress. *Acta Metallurgica*, 26(10):1579–1589, 1978.

[21] F. Larché and J. W. Cahn. A linear theory of thermochemical equilibrium of solids under stress. *Acta metallurgica*, 21(8):1051–1063, 1973.

[22] F. Larché and J. W. Cahn. A nonlinear theory of thermochemical equilibrium of solids under stress. *Acta Metallurgica*, 26(1):53–60, 1978.

[23] F. Larche and J. W. Cahn. The interactions of composition and stress in crystalline solids. *JOURNAL OF RESEARCH of the National Bureau of Standards*, 89(6):467, 1984.

[24] D. H. Lindsley. Some experiments pertaining to the magnetite–ulvöspinel miscibility gap. *American Mineralogist*, 66(7-8):759–762, 1981.

[25] C. Miehe, H. Dal, L.-M. Schänzel, and A. Raina. A phase-field model for chemo-mechanical induced fracture in lithium-ion battery electrode particles. *International Journal for Numerical Methods in Engineering*, 106(9):683–711, 2016.

[26] R. Milke, R. Dohmen, H.-W. Becker, and R. Wirth. Growth kinetics of enstatite reaction rims studied on nano-scale, part i: Methodology, microscopic observations and the role of water. *Contributions to Mineralogy and Petrology*, 154(5):519–533, 2007.

[27] R. Milke, R. Abart, K. Kunze, M. KOCH-MÜLLER, D. Schmid, and P. Ulmer. Matrix rheology effects on reaction rim growth i: evidence from orthopyroxene rim growth experiments. *Journal of Metamorphic Geology*, 27(1):71–82, 2009.

[28] K. Miyazaki. Ostwald ripening of garnet in high p/t metamorphic rocks. *Contributions to Mineralogy and Petrology*, 108(1):118–128, 1991.

[29] K. Miyazaki. A numerical simulation of textural evolution due to ostwald ripening in metamorphic rocks: A case for small amount of volume of dispersed crystals. *Geochimica et cosmochimica acta*, 60 (2):277–290, 1996.

[30] E. Moulas, Y. Y. Podladchikov, L. Y. Aranovich, and D. Kostopoulos. The problem of depth in geology: When pressure does not translate into depth. *Petrology*, 21(6):527–538, 2013.

[31] A. Nemchin, L. Giannini, S. Bodorkos, and N. Oliver. Ostwald ripening as a possible mechanism for zircon overgrowth formation during anatexis: theoretical constraints, a numerical model, and its application to pelitic migmatites of the tickalara metamorphics, northwestern australia. *Geochimica et Cosmochimica Acta*, 65(16):2771–2788, 2001.

[32] W. Noll, B. D. Coleman, and W. Noll. The thermodynamics of elastic materials with heat conduction and viscosity. *The Foundations of Mechanics and Thermodynamics: Selected Papers*, pages 145–156, 1974.

[33] M. Perez. Gibbs–thomson effects in phase transformations. *Scripta materialia*, 52(8):709–712, 2005.

[34] R. Powell, K. A. Evans, E. C. Green, and R. W. White. On equilibrium in non-hydrostatic metamorphic systems. *Journal of Metamorphic Geology*, 36(4):419–438, 2018.

[35] A. Sarmiento, L. Espath, P. Vignal, L. Dalcin, M. Parsani, and V. M. Calo. An energy-stable generalized-α method for the swift–hohenberg equation. *Journal of Computational and Applied Mathematics*, 344: 836–851, 2018.

[36] R. F. Sekerka and J. W. Cahn. Solid–liquid equilibrium for non-hydrostatic stress. *Acta materialia*, 52 (6):1663–1668, 2004.

[37] L. Tajčmanová, Y. Podladchikov, R. Powell, E. Moulas, J. Vrijmoed, and J. Connolly. Grain-scale pressure variations and chemical equilibrium in high-grade metamorphic rocks. *Journal of Metamorphic Geology*, 32(2):195–207, 2014.

[38] L. Tajčmanová, J. Vrijmoed, and E. Moulas. Grain-scale pressure variations in metamorphic rocks: implications for the interpretation of petrographic observations. *Lithos*, 216:338–351, 2015.

[39] C. Truesdell. Historical introit the origins of rational thermodynamics. In *Rational Thermodynamics*, pages 1–48. Springer, 1984.

[40] I. Tsagrakis and E. C. Aifantis. Thermodynamic coupling between gradient elasticity and a cahn–hilliard type of diffusion: size-dependent spinodal gaps. *Continuum Mechanics and Thermodynamics*, 29(6): 1181–1194, 2017.

[41] J. C. Vrijmoed and Y. Y. Podladchikov. Thermodynamic equilibrium at heterogeneous pressure. *Contributions to Mineralogy and Petrology*, 170(1):1–27, 2015.

[42] J. Wheeler. Dramatic effects of stress on metamorphic reactions. *Geology*, 42(8):647–650, 2014.

[43] X. Zhong, J. Vrijmoed, E. Moulas, and L. Tajčmanová. A coupled model for intragranular deformation and chemical diffusion. *Earth and Planetary Science Letters*, 474:387–396, 2017.